The Potential for Compact Helicon Wave Sources for Electric Propulsion*†

Jim Gilland
Ohio Aerospace Institute
NASA Glenn Research Center
Cleveland, OH 44142
440-962-3142
james.h.gilland@grc.nasa.gov

IEPC-01-210

The generation of plasma using a helicon plasma wave has been suggested as an electrodeless plasma propulsion concept. Plasma propulsion concepts impose geometric constraints on helicon wave generation that have not been widely investigated in most helicon sources. Specifically, short, narrow, high density plasmas would be required for most propulsion applications. The start up and attainment of high densities under these conditions may prove difficult. Initial experiments at the University of Wisconsin Madison have examined the use of a second pulsed, 1-3 kW 5 cm long helicon antenna on a 700 W steady state helicon discharge created by an 18 cm long antenna. The goal of these experiments is to increase the plasma density beyond the capability of the longer antenna. Results have shown an increase in density at the beginning of the high power pulse of 2-3 times. This initial increase does not remain constant, but decays to a lower value comparable to the steady state density over the course of the pulse. Neutral pumping effects are examined as a possible cause for this decay.

Introduction

Helicon Sources and Thruster Concepts

A helicon wave plasma source has several characteristics that might be beneficial to electric propulsion. It is an inductive plasma source, which eliminates the need for electrodes exposed to the plasma. It has been shown to be an efficient generator of high (~10^{19} m^{-3}) density, low (3-5 eV) temperature plasmas, primarily focused on plasma processing applications [1,2]. Because the helicon wave operates in a regime where the electrons are heated rather than ions ($\omega_{LH} > \omega \leq \Omega_e$, ω_{LH} = lower hybrid frequency, Ω_e = electron cyclotron frequency), the choice of propellant species does not directly affect the design parameters for the heating apparatus. Propellant choice will, of course, affect the overall performance of a thruster through frozen flow and line radiation losses. The robustness of the heating mechanism, in combination with the lack of electrodes, allows for the possible use of corrosive propellants such as oxygen.

Two immediate applications of helicon waves and discharges to electric propulsion are 1.) As a plasma source for electrostatic propulsion, and 2.) as both the plasma generation and heating mechanism in an electron cyclotron resonance thruster [3,4]. However, in both applications, a short axial wavelength and small transverse wavelength are desirable for a compact thruster design. This leads to an operating regime that may be difficult to initiate or maintain.

Helicon Wavelengths

Helicon waves have been found experimentally [5] to have "optimal" antenna lengths for maximizing density. Several interpretations of this phenomenon invoke a form of collisionless damping [6,7], particularly at low plasma densities during start up. In these interpretations, the wave phase velocity is

* Presented as Paper IEPC-01-210 at the 27th International Electric Propulsion Conference, Pasadena, CA, 15-19 October, 2001.

transferred to the electrons. The greatest densities are obtained when this phase velocity is matched to the peak velocity for electron impact ionization, which corresponds to an electron energy of 80 – 100 eV. [2,6]:

$$\frac{\omega}{\mathbf{k_z}} = \sqrt{\frac{2E_{\max}}{m_e}} \qquad \textbf{(1)}$$

where k_z is the propagation vector component parallel to the applied field.

A simplified helicon dispersion relation for azimuthal mode number m = -1,0,1 also shows that k_z is also determined by the plasma density if other parameters are kept constant:

$$\frac{B_0}{n_e} = \frac{\mu_0 e}{\mathbf{k}}\left(\frac{\omega}{\mathbf{k_z}}\right) \qquad \textbf{(2)}$$

where B_0 is the applied axial magnetic field, n_e is the plasma density, and **k** is the total wave propagation vector $\mathbf{k}=\sqrt{\mathbf{k_z^2}+\mathbf{k_\perp^2}}$. $k_\perp$ is the transverse (radial) component, usually expressed as $\mathbf{k}_\perp = \frac{Z_n}{a}$, with a the plasma radius and Z_n the nth zero of the J_0 Bessel function. For fixed ω and B_0, the two constraints above impose values of k_z that decrease as the density changes.

Most helicon experiments have been conducted in chambers on the order of 1-2 m long, .02 - .1 m diameter. In these experiments, the axial wavelengths are on the order of tens of cm, and the perpendicular wavelengths are a few cm. Then $k_\perp >> k_z$, k~ $k_\perp$, and equation 2 can be written as

$$\frac{B_0}{n_e a} = \frac{\mu_0 e}{Z_n}\left(\frac{\omega}{\mathbf{k_z}}\right). \qquad \textbf{(3)}$$

The Phaedrus helicon wave experiment at the University of Wisconsin-Madison fits in this category, with chamber length of 1.2 m, inner diameter 0.1m. In contrast, near-term propulsion applications might be expected to have axial dimensions of 10s of cm, and radial dimensions of 1-2 cm. This reduces the wavelength needed for helicon waves to propagate, requiring higher k_z values. However, for a constant frequency and plasma dimension, higher k_z drives the phase velocity away from the ionization constraint, making low-density plasmas harder to initiate.

For example, efficient ionization of argon gives a k_z value ~15 m^{-1} at a frequency of 13.56 MHz, which corresponds to a plasma density on the order of 1.2 x 10^{19} m^{-3} for an applied field of 0.1 T. The maximum density obtained in the UW helicon experiment using an antenna with wavelength of ~36 cm (k_z~17 m^{-1}) at the same frequency, with B_0=0.1 T, a~3 cm is n_e~ 1.2 10^{19} m^{-3}. By the dispersion relation, increasing the density to 5 x 10^{19} m^{-3} would require a k_z value of 60-70 m^{-1}. This gives a wavelength of ~0.05-.10 m, which is far from the value for collisionless ionization, and low on the power spectrum for a 30 cm wavelength antenna. The antenna that effectively launches helicon waves at low start up densities would also have to launch wavelengths five times lower to achieve higher densities. Alternatively, a second, shorter antenna could be used after startup to launch helicon waves at a higher k_z value. The power to bring the plasma to a higher density could be coupled more effectively with the shorter antenna. Coulomb collisional wave damping would be sufficient for further heating of the plasma [7].

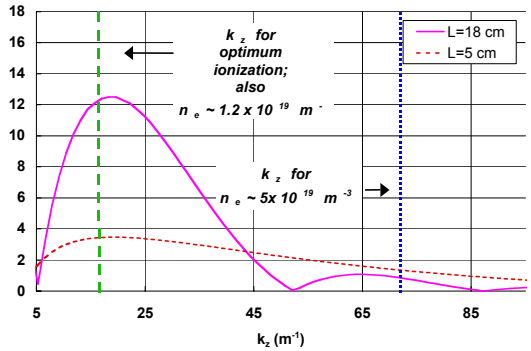

Figure 1 Effect of antenna size on vacuum spectra.

This use of two antennae optimized for different density regimes is shown in detail in Figure 1. In this figure, two vacuum spectra of antenna electric fields are shown, one for an 18 cm long antenna, and one for a 5 cm long antenna. These lengths correspond to wavelengths of 36 and 10 cm, respectively. The 18 cm antenna has a maximum field at k_z ~ 17 m^{-1}, close to the efficient collisionless ionization constraint. This also corresponds to the antenna used to initiate the Phaedrus helicon source and bring it to ~1 x 10^{19} m^{-3}. The 5 cm antenna has a broader spectrum, with a broad k_z peak, but a much lower maximum E-field. More importantly, the shorter antenna has a higher loading at k_z~70 m^{-1}, corresponding to a 5 x 10^{19} m^{-3} density that has not been achieved in the Phaedrus source. It should be noted that in initial experiments with the Phaedrus source, the shorter antenna was incapable of initiating a helicon wave plasma at 700 W. Another means of coupling at higher densities would be for higher order radial or azimuthal modes to

appear. Other experiments have primarily observed the presence of higher order radial modes [8, 9] .

Neutral Pumping

An additional effect that plays a role in determining plasma density is neutral pumping. This is the phenomenon that occurs as a result of the high plasma densities obtained in a helicon discharge. At electron temperatures (T_e) of 3-5 eV and a plasma density of 10^{19} m^{-3}, the ionization rate is higher than can be sustained at 10's of mtorr of neutral gas. Instead, "neutral pumping" occurs, where all the neutrals in the discharge are ionized until they escape the discharge at the end of the chamber where they recombine and are pumped out or reenter the discharge to be ionized again. During a steady state (700W) discharge, the neutral pressure measured at the edge of the plasma was 10% the value of the neutral pressure before the discharge was initiated. [10].

This neutral-depleted state is reached in 10 msec. or less, and can provide an upper limit to the density in a steady state helicon discharge. It has been proposed that the refueling rate of neutrals to the discharge in the center of the chamber is the limiting factor to achievable helicon density [11]. This observation arose from an experiment similar to the one described here, with two antennae operating simultaneously. Instead of increased density, a decrease in density was observed, particularly in the region between the two antennae. This was ascribed to neutral pumping effects. However, the experiment used two antennae of equal length, which also allowed for the limitation of the antenna coupling at high densities. [11]] The attempt of this experiment has been to try and separate the two possible limiting effects.

The Dual Antennae Helicon Experiment

The helicon source at the University of Wisconsin-Madison has generated plasma densities in argon up to 3 x 10^{19} m^{-3}, at electron temperatures of 3-5 eV, using less than 1 kW of 13.56 MHz rf power. The experimental apparatus is shown in Figure 2. The discharge chamber is a Pyrex tube 120 cm long, 10 cm inner diameter. Solenoidal coils along the length of the chamber generate an applied axial magnetic field of 0.1 T. The end coils have the capability to reverse the current direction, allowing cusped fields at either end of the chamber. A cusped magnetic field configuration has been found to improve confinement in some helicon discharges [5]. Results discussed in this paper are all for an uncusped magnetic field.

The chamber is closed at both ends, with pumping and gas feed at the same end of the chamber to minimize pressure gradients in the discharge. The source is typically operated with pre-discharge neutral pressures of 5 - 30 mtorr. Pressure is measured using a Baratron capacitive manometer installed at the far end of the chamber from the pump and gas feeds. The capacitive manometer is not affected by rf fields from the discharge.

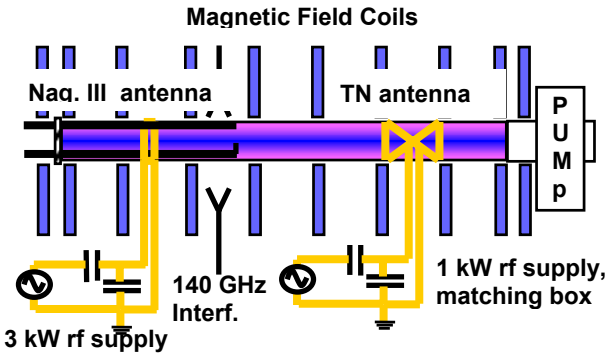

Figure 2. University of Wisconsin Phaedrus helicon experiment.

The experiment currently has two copper-strap antennae installed on it, with two separate power supplies. The two antenna designs used are shown in Figure 3. The right hand antenna in Figure 3 is the low power, steady state antenna, which is called a "Twisted Nagoya" (TN) antenna for the helical winding of the axial straps. This antenna is 18 cm long for more efficient collisionless coupling to the plasma at low densities. The antenna is operated at 700 W of rf power at a frequency of 13.56 MHz. The helical design of this antenna allows it to selectively launch an m=+1 mode wave down the length of the chamber. The power source is a PlasmaTherm 1 kW system. A capacitive matching circuit was constructed that allows powers up to 1 kW with less than 20 W reflected power.

The left hand antenna is a "Nagoya III" (NIII) design, 5 cm long, which can be operated in pulsed mode up to 3 kW at frequencies of 10-20 MHz. This antenna is powered by a Tektronix signal generator feeding an ENI 500A and Henry 5K rf amplifiers to produce powers up to 3 kW in short pulses. A capacitive matching circuit was also used to allow pulses with

less than 30W reflected power. A frequency of 13.56 MHz was also used in these experiments for the second antenna. This antenna launches both m=+1 and –1 waves in both axial directions. Because the coupling to the m=-1 is bad for helicon waves, and because the antenna launches the +1 mode in both directions, its loading on the plasma will generally be worse than that of the Twisted Nagoya. However, this antenna does allow for the possibility of launching m=-1 waves at higher densities, which has not yet been observed in these devices.

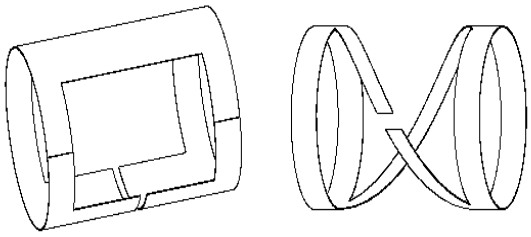

Figure 3. Antenna designs for this experiment. Left: Nagoya III. Right: "Twisted Nagoya".

Diagnostics

Diagnostics for the two antenna experiment have currently focused on density measurements. An rf compensated Langmuir probe is inserted into the discharge chamber on an axial shaft, with a dogleg bend at the end to allow for radial density profiles. The probe itself is a graphite cylinder, 0.5 mm diameter, 1 mm long. The small size and graphite composition are to minimize probe sputtering and heating in the high density plasma. Compensation is provided by two LC resonant circuits tuned to reject both 13.56 MHz and 27 MHz fluctuations in plasma potential, and give a more accurate measurement of electron temperature. For the density measurements presented here, the probe was biased at –140 V to measure ion saturation. The high bias voltage was necessary to eliminate large current fluctuations in the ion saturation signal during the high power pulse.

The Langmuir probe was primarily used for obtaining radial and axial plasma density profiles in the low power steady state plasmas. It was found that the probe perturbed the plasma at high powers in two ways. First, the probe reduced the interferometer signal by up to 20% when located within 2 cm radially of the high density center of the plasma. Second, the probe introduced some form of contamination when located in the high density region, which degraded the discharge after approximately 10 discharges. Similarly, a triple probe has also been installed on the experiment for real time Te measurements; however its use has been limited due to concerns of similar plasma contamination or perturbation of the discharge.

An alternative density measurement was obtained using a 140 GHz microwave interferometer. This measures line-averaged densities across the diameter of the discharge. A heterodyne signal method is used to process the signal [12], and the phase shift output is digitized at a rate of 100 KHz. Comparison of the probe density profiles and interferometer signals showed close agreement, with the interferometer response following that of the centerline density measured by the probe. Increases in plasma diameter are a second order effect in the interferometer measurements. The interferometer is located in a fixed axial position 17 cm from the center of the Nagoya III antenna, and 46 cm from the center of the steady state TN antenna.

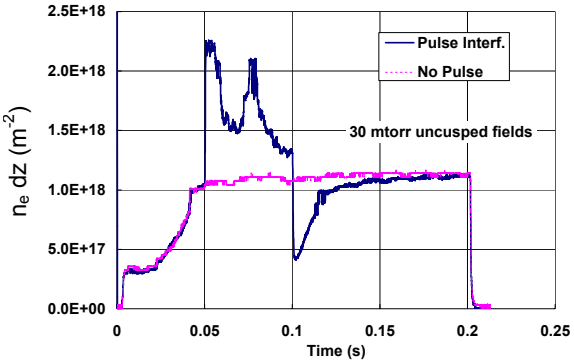

Figure 4. Plasma response measured by interferometer for 2.8 kW 30 mtorr pulse.

Operation

The system is operated in a two-pulse manner. The low power source is matched for initiating a plasma at 700 W, over a 200 msec. pulse. The high power system is tuned to match to the plasma while the low power system is on. During a data shot, the 700 W system is turned on, then the high power, shorter antenna is pulsed for 50 msec., beginning 50 msec. after the initiation of the low power system. A representative shot as measured by interferometry is shown in Figure 4. Because of Langmuir probe perturbation effects during the pulsed operation, the probe was rotated out to the edge of the plasma for

most of the experiments, where it had no effect on interferometer measurements.

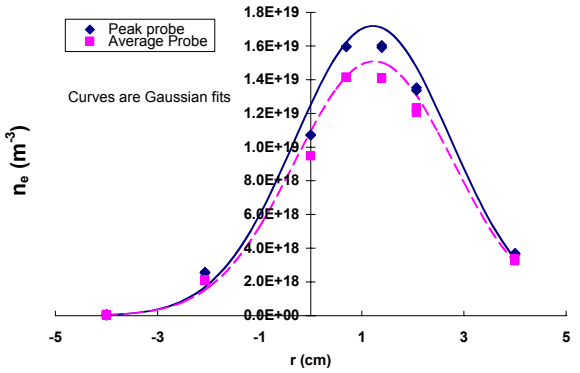

Figure 5. Experimental electron density profiles 23 cm away from TN antenna for the Phaedrus helicon source at 0.1 T, 10 mtorr, 700 W rf power.

The 700 W plasma density profile measured by a rf-compensated Langmuir probe is shown in figure 5. The applied field was 0.1 T and rf power was 700 W and the probe was 23 cm away from the center of the TN antenna. Other experiments have found that the axial location for the peak density for a single antenna occurs approximately 2 to 3 antenna lengths away from the center of the antenna [13]; this probe location was as near as possible to that maximum location. Two sets of data are shown: the density values during the period when a high power pulse would occur ("Peak Density"), and the values in the steady state portion of the pulse after the pulse is over, ~ .18 msec. into the pulse ("Average Density"). The curves are gaussian fits to aid the eye. The off-center peak has been seen in many experiments [1,10], and may be a result of the Langmuir probe perturbation.

The T_e profile has been measured previously [10] and found to be essentially constant across the radius of the discharge. Due to the pulsed nature of this work, and the probe perturbation effects, swept probe traces to determine T_e were determined to be infeasible. Future work with a triple probe will be performed to determine T_e profiles in the plasma during the high power pulse. The plasma half width at half maximum (HWHM) is **a** ~ 2 cm.

The scaling of peak density with rf power for the steady state helicon discharge with a single 30 cm wavelength antenna is shown in figure 6. An abrupt jump in plasma density can be observed at about 250 W, which corresponds to the appearance of a bright blue-white central column in the discharge, indicative of increased ionization. The density reaches an asymptotic value at high powers, due to plasma losses at the boundaries. The measured peak densities and plasma dimension (**a**) follow the dispersion relation (equation 2) if the wavelength is assumed to be determined by the antenna length, $\lambda \sim 30$ cm. The resulting phase velocity is close to the E_{max} for argon, ~ 80 eV.

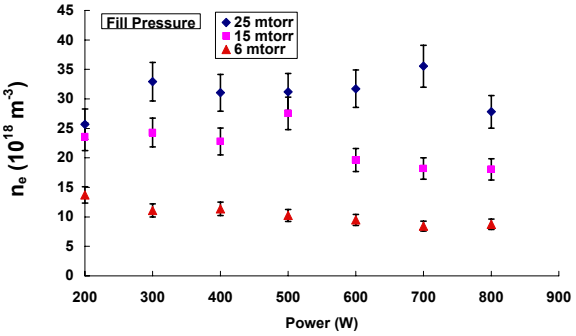

Figure 6. Scaling of electron centerline density with rf power and pressure, 16 cm from TN antenna centerline.

Dual Antennae Results

Pulse waveforms

Sample interferometer traces averaged over 3 shots of the dual antenna system operating with a 700 W, 0.2 sec steady state pulse and a 50 msec, 2.8 kW high power pulse are shown in Figure 7 for pre-discharge pressures of 5, 10, 20, and 30 mtorr. The scales of all figures are the same, to allow direct comparison of the peak and average line averaged density magnitudes for each pressure. The corresponding trace for the 0.2 sec 700 W pulse is also shown for comparison in each figure. Figure 8 shows a similar progression of pulse waveforms for increasing pulsed rf power levels of .84, 1.5, 2.3 and 2.8 kW at a constant fill pressure of 20 mtorr. At the highest power and pressure measured here, 2.8 kW and 30 mtorr, the monotonic behavior of the line-averaged-density ceases and a second peak appears. Some indication of a second peak partially forming at 2.8 kW and 20 mtorr may also be seen.

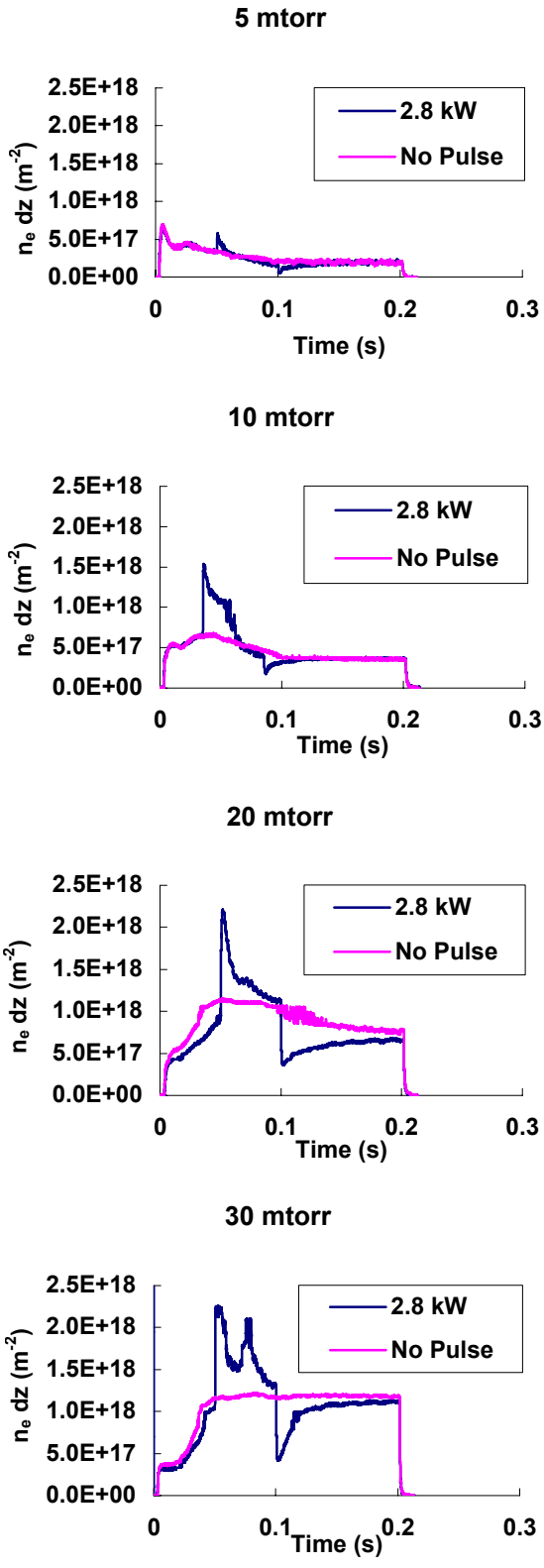

Figure 7. Line-averaged density behavior for increasing pressure.

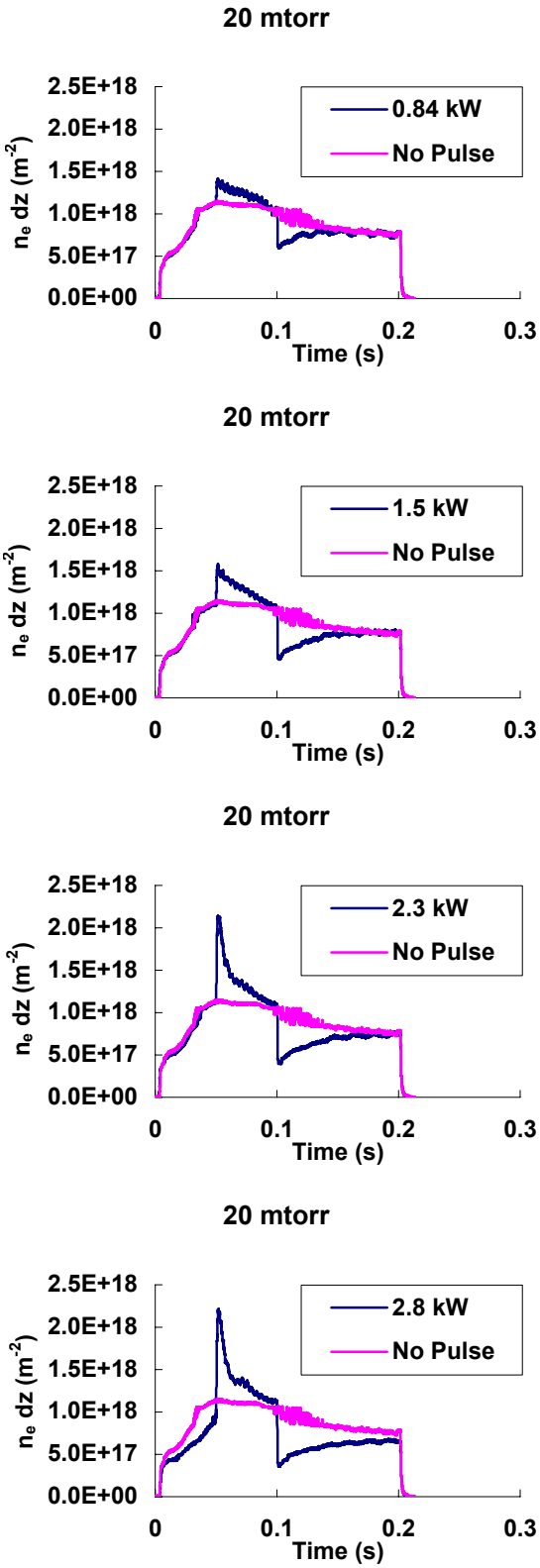

Figure 8. Line averaged density for increasing pulsed power.

The temporal behavior during the pulse is qualitatively similar for each pressure. The pulse begins with a rapid increase in density, followed by a density decay extending over the pulse length. The initial peak rapidly decays, but then slows as it approaches density values comparable to the steady state value. It should be noted that the pulse forms for 10 mtorr data exhibit slightly different behavior than for pressures above or below. Specifically, a slow decay from the peak with a sharp transition in mid-pulse, followed by another slow decay. Similar behavior is also seen after the end of the pulse: a fast drop in density below steady state levels as the power is turned off, followed by a slower recovery to the steady state value. At high powers, the recovery period also exhibits two time scales.

Line-Averaged Plasma Density

In order to quantify the effects of varying pulse powers and fill pressures on the efficacy of the second antenna in increasing plasma density, the interferometer values at several representative times during the discharge have been selected for comparison, as well as some ratios of these values. Absolute measurements of interest are the peak density at the beginning of the high power pulse ("peak"), the density at the end of the pulse ("end"), the density undershoot at the end of the pulse ("dip"), and the density at the end of the steady state discharge ("steady-state"). Data points are averages for at least 3 shots at a given condition. The error bars are the standard deviation of the shots, and indicate repeatability of the measurement rather than experimental error.

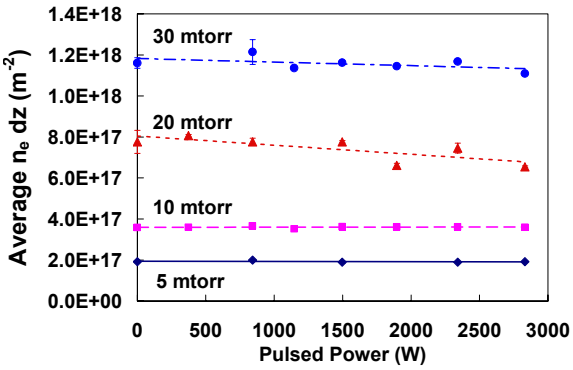

Figure 9. Steady-state line-averaged density generated by 18 cm, 700 W antenna over a range of pressures after high power pulse.

Steady-State Line-Averaged Density (Figure 9) The density measured well after the cessation of the high power pulse is essentially independent of the pulsed power, as would be expected. There is a slight decrease in the steady-state value at higher power levels, due to the greater time required for the plasma to recover after the pulse has turned off. The steady-state density scales linearly with pressure increasing from 1.9 x 10^{17} m^{-2} at 5 mtorr to 1.2 x 10^{18} m^{-2} at 30 mtorr. This linearity with pressure suggests that the low power plasma densities are governed by the availability of neutrals to be ionized by the wave-heated electrons. It should be noted that previous single antenna experiments with a range of pressures all reached an asymptote in plasma density with increasing rf power [11], which suggests that the limits are at least partially due to neutral refueling limitations in the discharge.

Peak Line-Averaged Density (Figure 10) The sensitivity of the initial peak in the high power pulse to pulse power varies with pressure. The effect of the second antenna at 5 mtorr is low. The density increases appreciably with power at 10 mtorr and higher. Peak density values at pressures above 20 mtorr coverge at high power to a value on the order of 2.2 x 10^{18} m^{-2}. This is about twice the peak density with the single antenna at a power level that is four times greater. Unilike measurements done at higher pressures with the single longer antenna, the peak density continues to increase with power at high pressures. This could imply better coupling of the shorter antenna to the high density plasmas, although further measurement of wave properties during the pulse will be required to verify this.

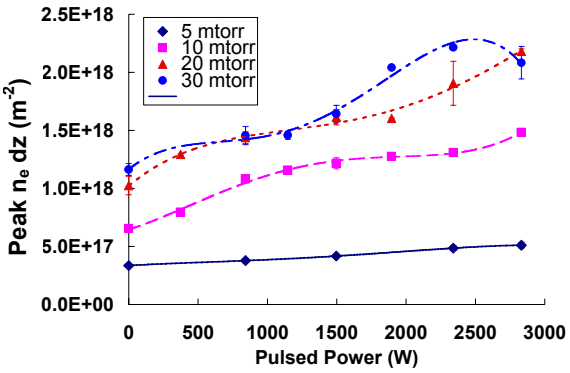

Figure 10. Initial peak line-averaged density at start of high power pulse for 5-30 mtorr.

End Line-Averaged Density(Figure 11) End density, that is the plasma density at the end of the high power pulse, shows a marked bifurcation in behavior with respect to fill pressure. At pressures below 20 mtorr, the end pressure is independent of power and scales much like the average density with pressure. At 20 mtorr or above, end density is higher than average density by 30% (20 mtorr) to 20% (30 mtorr). Two effects may be ocurring to determine this behavior.

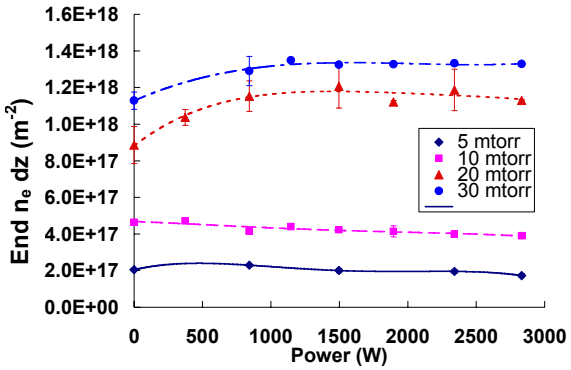

Figure 11. The line-averaged density at end of the high power pulse is more sensitive to power at high pressures.

First, at low pressures the plasma density (2 – 4 x 10^{17} m^{-2} line averaged) may be too low to allow effective coupling of the second antenna to the plasma. Second, the lower number of available neutrals in the low pressure discharges may not provide enough fueling for additional ionization. The first hypothesis could be tested by examining the forward power to the antenna to determine coupling. The second hypothesis might result in a rise in T_e as more energetic electrons are produced to ionize the few neutrals that remain. Both options will be examined in future work by measuring forward power with an rf power meter and T_e with a triple probe in the center of the discharge.

Density "Dip"(Figure 12) At the end of the high power pulse, the plasma density quickly drops *below* the steady state value, even though the 700 W antenna is still operating. This minimum density value is shown in figure 12. This would appear to be a purely fluid effect, since there is no issue of the longer antenna coupling to the steady state value of the plasma. The density undershoot scales similarly to the peak density: weak power dependence at low pressure, stronger power dependence at high pressure, but reaching an asymptotic value at the highest pressures and power. The absence of pulsed antenna coupling issues in this regime implies that the behavior is primarily related to neutral flow in the discharge.

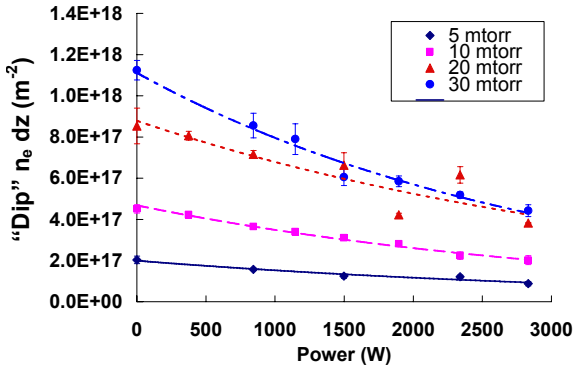

Figure 12. Line-averaged density at minimum "dip" immediately after end of high power pulse.

The relationship between the peak and dip densities is shown more fully in terrms of their ratio (Figure 13). The curves shown are exponential fits to the data. With the exception of 10 mtorr, the ratio is essentially pressure independent, ranging from 1.5 to 5 over the power range. The magnitudes of the peak and dip scale identically with pressure, but the relative magnitude of the peak to the dip increases somewhat with power. This indicates that while the values of peak and minimum densities diverge, the divergence is not determined by the fill pressure.

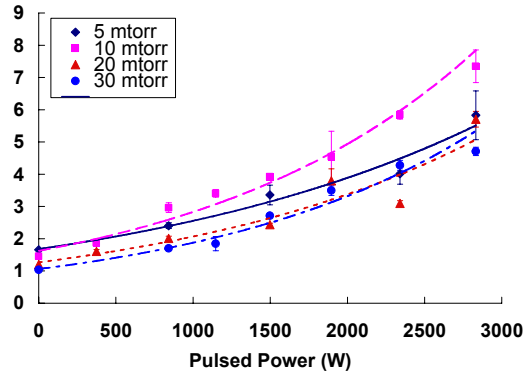

Figure 13. The relationship between peak and minimum line-averaged densities is essentially independent of pressure.

Pulse Time Scales

Several time scales appear in the pulse waveform. At the start of the pulse, a fast decay from the peak

value occurs, followed by a slower decay over the last half of the high power pulse. Immediately after the pulse ceases, there is a slow recovery from the dip value to the steady-state value. All three of these time scales have been estimated by fitting the respective time segments of the interferometer data to exponential functions. The variation of these times with power and pressure are shown in Figures 14-16.

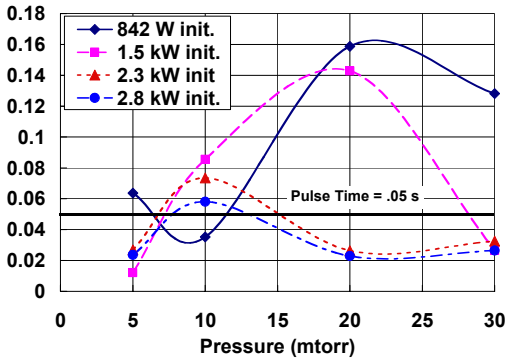

Figure 14. Initial decay times show bifurcation at high pressures and power.

Initial decay time The initial decay from the peak value at the beginning of the pulse is shown in figure 14. For comparison, the duration of the pulse itself, 50 msec, is also given. The curves are given to help the eye. These calculations are shown versus pressure, with equal-power curves ranging from 0.84 to 2.8 kW. Time scales at low pressures show similar behavior, with the exception of the lowest power curve, which is reversed in behavior. For powers $\geq$ 1.5 kW, time scales are comparable at 5 mtorr then increase to 1.2 to 2 times the pulse length at 10 mtorr. At higher pressures, the time scales divide into low ($\leq$ 1.5 kW) and high ($\geq$ 2.3 kW) power regimes. At low power, the decay times extend to be greater than the pulse time. At high power, the time scales decrease to about .02 sec., independent of power level 1.5 kW actually appears to be a "cross over" point between the two regimes, with the time at 20 mtorr comparable to that at 5 mtorr, but the time at 30 mtorr comparable to the high power time scale.

Looking at this phenomenon in another way, there appears to be a threshhold density-power combination that determines the decay times. In figure 15, the initial decay time is plotted against peak density. At a value of approximately 1.3 x 10^{18} m^{-2}, two branches in the decay time appear, a low power and a high power one. The low power branch shows a sharply increasing decay time, while the high power branch reaches a maximum time on the order of 0.065 sec., then decreases to a value of ~ .025 sec., indicating a more rapid decay for higher peak densities at higher power, regardless of pressure.

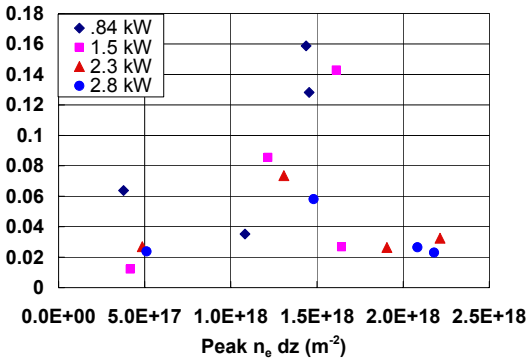

Figure 15. Decay time scales immediately after the peak density showing thresholds in density and power determining decay rate.

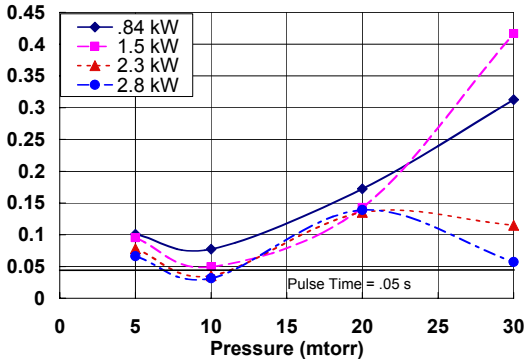

Figure 16. End decay time scales show that density decay is somewhat insensitive to power level. Differences at higher power/pressure may be due to the presence of a second density peak in mid-pulse.

End decay time The decay time later in the pulse, as opposed to immediately after the peak density of the pulse, is slower, and scales differently with pressure, and power, as shown in figure 16. This time scale is essentially independent of power for pressures $\leq$ 20 mtorr. With the exception of 10 mtorr, in which the

pulse shape has a sharp density drop in the middle of the pulse, time scales are longer than the pulse time. The general increase in time with pressure indicates improved refueling at the higher pressures, but that the initial high density peak establishes the deficiency to be refilled.

Actually, the divergence at 20 and 30 mtorr is most likely due to the the change in pulse shape at the high power and pressure, with 2.3 and 2.8 kW pulses producing multiple peaks during a single pulse. The time scales given here were based on the decay after the second peak. While they are not as short as the initial decay times, the sudden decrease in decay time is most likely due to the second high density peak that occurs in the pulse.

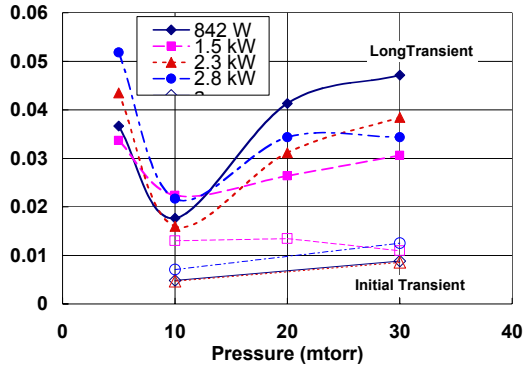

Figure 17. Plasma density recovery times after cessation of high power pulse are most strongly affected by pressure.

Post-pulse recovery time In addition to a high power decay, the plasma also exhibits a slow rise time after the pulsed power is turned off. In some cases a fast initial recovery is followed by a slower one. The two phases are not evident in every case. Specifically , pressures of 10 mtorr and 30 mtorr have two time scales. Both scales are shown in figure 17: the slower time scales are the solid symbols, while the faster initial time scales are the hollow symbols. The fast scales range from 7 to 13 msec, while the slower scales are 30 – 50 msec. An examination of the pulse waveforms suggest two different reasons for the long time scales. At the lowest pressure, the time scales are long because the minimum density is close to the average density, and what looks like a long transition is actually just the fact that the values are so close. At high pressures, the dip is much lower than the average, and recovery is longer as a result. Also, the higher powers have a faster recovery initially, which brings the density to a state that can recover at the slower rate over the remainder of the pulse.

Discussion and Summary of Results

Plasma Density Scaling In terms of the goal of increasing density, the brief peak density at the start of the pulse indicates that the smaller antenna can increase plasma density over the limiting value of the longer antenna, but only briefly. Significant increases in density (two or three times) over the steady state densities require pulsed powers equal to or greater than the baseline power of 600 W, and pressures of 10 mtorr or higher. However, pressures beyond 30 mtorr and powers beyond 2 kW (> 3 times the steady state power level) yield diminishing returns in density.

The end density appears to approach the density values obtained with the steady state antenna and power, which could imply that the shorter, high power antenna is not effectively coupling to the plasma. However, reflected power values are less than 30 W over the course of the discharge. Furthermore, the sharp plasma density decrease after the pulse, and its scaling with peak density with only a weak dependence on pressure indicates that some additional ionization is taking place during the pulse.

It is interesting to note that at 30 mtorr, and pulsed power levels ≥ 2.3 kW, a second plasma peak appears during the course of a single pulse. A similar behavior was observed by Degeling, et al. in a lower field, high power source using a single antenna [14]; however, the time scales in that experiment were ~5 msec., rather than the ~20 msec. observed here. Degeling et al. proposed a relaxation from a high density, helicon wave coupled plasma to a lower density, inductive plasma, invoking neutral pumping as the cause of the change of state. While neutral pumping and antenna coupling undoubtedly play a role in this experiment as well, additional processes are also present due to the multiple antennae. For example, lower pulsed power or pressure cases of the multiple antenna system reach and pass through the same low density values seen at high powers without the appearance of a second density peak. A balance between neutral refilling at higher pressures and the ionization rate at the higher

powers must be satisfied to produce the second high density cycle.

Plasma Response Several processes seem to influence the plasma formation during and immediately after the high power pulse from the shorter antenna. Power and pressure play different roles in these processes, as evidenced by the different dependencies observed. Thresholds in power and pressure appear to exist to divide plasma response between slow and fast decay rates.

The decay in the peak density is strongly governed by the fill pressure, which implies a neutral pumping limit. Miljak and Chen calculated a limiting density based on neutral flow rates and derived an expression for a neutral density decay time [11]:

$$\tau_n = \frac{2R^2}{a\,\mathbf{v}_t} \qquad (4)$$

with R = chamber radius, a = plasma radius, and v_t = neutral thermal speed. For the Phaedrus experiment, R= .05 m, a ~ .02 m, and v_t ~ 300 m/s, giving a τ_n of 0.8 ms. This is a faster time scale than is observed over much of the pulse, although it is closest in magnitude to the initial decay of the pulse.

While the fast initial decay and recovery times may be related to the neutral depletion by ionization, before resupply of neutrals can be established, the basis for the longer time scales is less clear. In these longer periods, a particle and energy balance between neutral resupply and continued ionization by the 700 W antenna introduces competing processes, which are governed by the ionization rate, electron temperature, neutral flow, and the collisionality of the flow. The primary dependence of the long scale times on pressure underscores the importance of the resupply on this phase of the plasma response.

Conclusions

As a means of creating compact, high density plasmas, the use of a second, shorter antenna to launch helicon waves which couple to higher density plasmas shows some possibility of increasing density. However, neutral fueling and coupling issues remain, as do many unknowns about the process. A shorter antenna has been observed to briefly generate increased plasma densities which it could not achieve when used as a single antenna system. Neutral fill densities ≥ 10 mtorr are required for density increases on the order of 1.5 to 2 times that attained with a longer antenna. The increase in density also reaches an upper limit of approximately twice the longer antenna density (at comparable pressures). Power levels beyond 2 kW and pressures greater than 20 mtorr do not result in further density increases.

Several unknowns that remain to be determined in future experiments are the electron temperature response to the second antenna or, alternatively, the possible presence of high energy electron beams during the high power pulse that may generate or maintain increased densities with decreased neutral populations. These measurements will provide insight into modeling of the power and particle balance in the helicon discharges. Secondly, measuring the nature of the wavelengths propagating at different times over the course of the pulse will give information on the coupling of the smaller antenna to the plasma, and the variation of the wavelength as the plasma density changes throughout the pulse.

The presence of multiple peaks in plasma density at high power and pressure introduce the possibility of a repetitively pulsed plasma that might attain high average density values. Based on this initial data, pulses on the order 10 msec. with a duty cycle around 50%, could allow neutral refueling sufficient to produce repeated high density peaks. However, from a propulsion standpoint, pulsed operation of rf supplies and propellant feed systems may introduce complexity and inefficiency that mitigate the gains in density.

Acknowledgements

The author wishes to thank Prof. Noah Hershkowitz of the University of Wisconsin-Madison for his support of this research and his contributions to the work through discussions and reviews. The experimental work described in this paper was funded by NSF grant No. ECS-9529565.

References

[1] R.W. Boswell "Very Efficient Plasma Generation by Whistler Waves Near the Lower Hybrid Frequency,"

Plasma Physics and Controlled Fusion, **26**(10) p. 1147-1162. (1984).

[2] F. F. Chen, "Ionization by Helicon Waves," *Plasma Phys. and Controlled Fusion* **33**, 339 (1991).

[3] E. B. Hooper et al. "Analysis and Experiments of a Whistler-Wave Plasma Thruster," UCRL-JC-114643 LLNL Preprint, August 1993.

[4] J. H. Gilland. and N. Hershkowitz, "Application of a Helicon Discharge to Electric Propulsion," AIAA Paper No. 98-3934, 1998.

[5] Chen, F. F. "Experiments on helicon plasma sources," *J. Vac. Sci. Technol. A.* **10**(4) 1992.

[6] A. W. Degeling et al, "Plasma production from helicon waves," *Phys. Plasmas* **3** (7), 1996.

[7] F. Chen and D. Blackwell, "Upper Limit to Landau Damping in Helicon Discharges," *Phys. Rev. Lett.* **82** (13), 1999.

[8] R. T. S. Chen, et al., "Experimental Studies of Multimode Helicon Plasma Waves." *Journal of Plasma Sources Sci. Tech.*, Feb. 1995.

[9] M. Light, et al., "Axial propagation of helicon waves," *Phys. Plasmas* **2** (11), 1995.

[10] J. Gilland, R. Breun, and N. Hershkowitz, "Neutral pumping in a helicon discharge," *Plasma Sources Sci. Technol.* **7** (3) 1998.

[11] D. Miljak, and F. Chen, "Density limit in helicon discharges," *Plasma Sources Sci. Technol.* **7** (4) 1998.

[12] I. Hutchinson, *Principles of Plasma Diagnostics*, Cambridge:Cambridge University Press, 1987.

[13] F. Chen, I. Sudit and M. Light, "Downstream physics of the helicon discharge," *Plasma Sources Sci. Technol.* **5** 1996.

[14] A. Degeling et al., "Intense on-axis plasma production and associated relaxation oscillations in a large volume helicon plasma source, "*Phys. Plasmas* **6** (9) 1999.